Coherence-based photoacoustic imaging of brachytherapy seeds implanted in a canine prostate

Muyinatu A. Lediju Bell[a], Danny Y. Song[b], and Emad M. Boctor[a,c]

[a]Johns Hopkins University, Department of Computer Science, Baltimore, MD, USA;
[b]Johns Hopkins University, Department of Radiation Oncology, Baltimore, MD, USA;
[c]Johns Hopkins University, Department of Radiology, Baltimore, MD, USA

ABSTRACT

Visualization of individual brachytherapy seed locations assists with intraoperative updates to brachytherapy treatment plans. Photoacoustic imaging is advantageous when compared to current ultrasound imaging methods, due to its superior sensitivity to metal surrounded by tissue. However, photoacoustic images suffer from poor contrast with insufficient laser fluence. A short-lag spatial coherence (SLSC) beamformer was implemented to enhance these low-contrast photoacoustic signals. Photoacoustic imaging was performed with a transrectal ultrasound probe and an optical fiber surrounded by a light-diffusing sheath, placed at a distance of approximately 4-5 mm from the location of seeds implanted in an *in vivo* canine prostate. The average energy density through the tip of the sheath was varied from 8 to 167 mJ/cm^2. When compared to a fast Fourier transform (FFT)-based reconstruction method, the mean contrast and signal-to-noise ratios were improved by up to 22 dB and a factor of 4, respectively, with the SLSC beamformer (12% of the receive aperture elements were included in the short-lag sum). Image artifacts that were spatially coherent had spatial frequency spectra that were quadrantally symmetric about the origin, while the spatial frequency spectra of the seed signals possessed diagonal symmetry. These differences were utilized to reduce artifacts by 9-14 dB after applying a bandpass filter with diagonal symmetry. Results indicate that advanced methods, such as SLSC beamforming or frequency-based filters, hold promise for intraoperative localization of prostate brachytherapy seeds.

Keywords: ultrasound, photoacoustic imaging, optoacoustic imaging, FFT-based reconstruction, spatial coherence, frequency spectrum, filtering, beamforming, contrast, signal-to-noise ratio

1. INTRODUCTION

Brachytherapy is administered by permanently implanting approximately 50-100 radioactive seeds according to a predefined treatment plan.[1,2] Although transrectal ultrasound imaging is currently used for intraoperative visualization of prostate brachytherapy seeds, they are often difficult to locate due to factors like their small size, acoustic clutter, and multiple sound reverberations in the presence of many seeds. Photoacoustic imaging is being investigated as an alternative imaging method, due to the superior image contrast of metal surrounded by tissue, when compared to the corresponding acoustic contrast.[3–5] Photoacoustic imaging relies on laser light illumination and the subsequent optical absorption, thermoelastic expansion, and emission of sound waves that are detectable with an ultrasound transducer.

One limitation of photoacoustic imaging is the diminishing seed contrast with decreasing laser fluence. Another limitation is the presence of background noise that limits the usable dynamic range of an image. While there are several approaches to overcome these limitations (e.g. alteration of the seeds to increase optical absorption, decreasing the distance between the seed and light source[6,7]), amplitude-dependent photoacoustic reconstruction methods are a primary source of these limitations. Two of the most common amplitude-dependent reconstruction methods are delay-and-sum beamformers and fast Fourier transform (FFT)-based reconstruction.[8–10]

We previously demonstrated that photoacoustic images created with the short-lag spatial coherence (SLSC) beamformer are independent of signal amplitude, and thus have relatively constant contrast in the presence of

E-mail:muyinatu.ledijubell@jhu.edu

Medical Imaging 2014: Ultrasonic Imaging and Tomography, edited by Johan G. Bosch, Marvin M. Doyley, Proc. of SPIE Vol. 9040, 90400Q · © 2014 SPIE
CCC code: 1605-7422/14/$18 · doi: 10.1117/12.2043901

decreasing laser fluence.[11–13] It is less susceptible to insufficient laser energies because it measures and displays the spatial coherence of a received acoustic wavefield. The SLSC beamformer was compared to a conventional delay-and-sum beamformer to enhance visualization of brachytherapy seeds implanted in *ex vivo* and *in vivo* canine prostates.[12,14] This paper is the first to present the photoacoustic image quality improvements achieved when the SLSC beamformer is compared to a conventional FFT-based reconstruction method.

2. METHODS

A 25 kg dog was prepared for a prostate brachytherapy procedure approved by the Johns Hopkins Animal Care and Use Committee, as described in detail in our previous publication.[12] The dog was positioned supine with its legs and tail immobilized for unobstructed access to the perineum. A standard Nucletron stepper attached to a template guide were utilized for transperineal insertion of 18G brachytherapy needles. Non-radioactive, decayed ($>$ 10 half lives) brachytherapy seeds were surgically implanted through the hollow bore of the brachytherapy needle. The seeds were coated with black India ink to enhance optical absorption. The dimensions of the cylindrical seeds were 0.8 mm (outer diameter) x 4.5 mm (length).

A light-diffusing sheath was stiffened by inserting a temporary metal rod into the sheath lumen, and the sheath was inserted through the perineum, into the prostate, at a distance of approximately 4-5 mm from the implanted seeds. The temporary rod was removed and a 1-mm core diameter optical fiber with one end air-coupled to a 1064 nm Nd:YAG laser was inserted into the light diffusing sheath. This procedure was performed under transrectal ultrasound guidance. A SonixTouch ultrasound scanner (Ultrasonix, Richmond, BC, Canada) was connected to a transrectal ultrasound probe with curvilinear (BPC8-4) and linear (BPL9-5/55) arrays, and a data acquisition unit (SonixDAQ) for synchronized laser light emission and photoacoustic signal acquisition. The sample acquisition rate of the SonixDAQ was 40 MHz. B-mode ultrasound images were acquired with the same transducer and ultrasound system.

FFT-based reconstruction and a coherence-based SLSC beamformer were applied independently to the received photoacoustic signals. The FFT-based method was implemented using the k-Wave toolbox.[15] The SLSC photoacoustic images were calculated using the following equations:[16]

$$\hat{R}(m) = \frac{1}{N-m} \sum_{i=1}^{N-m} \frac{\sum_{n=n_1}^{n_2} s_i(n) s_{i+m}(n)}{\sqrt{\sum_{n=n_1}^{n_2} s_i^2(n) \sum_{n=n_1}^{n_2} s_{i+m}^2(n)}} \tag{1}$$

$$R_{sl} = \sum_{m=1}^{M} \hat{R}(m) \tag{2}$$

where $\hat{R}$ represents the normalized spatial correlation of received signals, m is the distance (i.e. lag) between two elements of the receive aperture in units of number of elements, R_{sl} is the short-lag spatial coherence, N is the total number of elements in the receive aperture, $s_i(n)$ is the time-delayed, zero-mean signal received by the ith element, n is the sample depth in units of samples, and M is number of lags included in the short-lag sum. The value of $n_2 - n_1$ was equivalent to the smallest wavelength within the bandwidth of the linear array (i.e. 0.308 mm). The value of M was set to 4, which corresponds to 12% of the number of elements in the receive aperture.

After applying the SLSC beamformer or FFT-based reconstruction, contrast was calculated as $20log_{10}(S_i/S_o)$, and the signal-to-noise ratio (SNR) was calculated as S_i/σ_o, where S_i and S_o are the means of the image data within regions of interest (ROIs) located inside and outside of the brachytherapy seed, respectively, and σ_o is the standard deviation of the data within the ROI located outside of the seed. Rectangular ROIs surrounding the maximum signal from the seed were manually selected for each seed in each image evaluated, and a matching ROI at the same depth and with the same size was automatically created, starting at a fixed lateral position to the right of the seed. The fixed lateral position was the same in paired SLSC and FFT-based images.

Beamformed and reconstructed data from the same photoacoustic signals were envelope-detected, normalized to the brightest image pixel, log compressed, and displayed with the same dynamic range. No frame averaging was applied to display images or calculate the image performance metrics (i.e. contrast and SNR). All image processing was performed with MATLAB software (The MathWorks, Inc., Natick, MA).

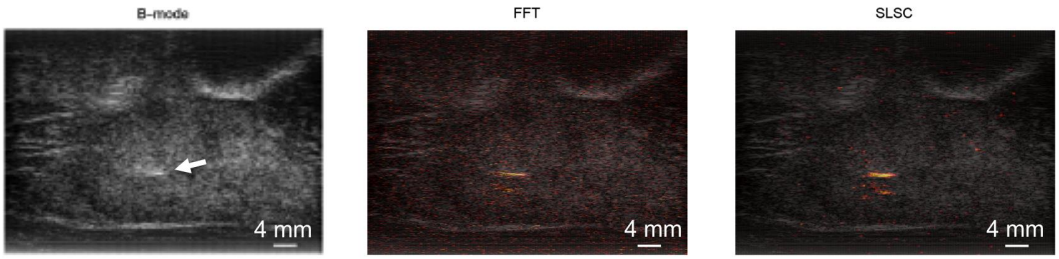

(a) (b) (c)

Figure 1. (a) A single brachytherapy seed (arrow) in an ultrasound B-mode image. Photoacoustic images formed with (b) FFT-based reconstruction and (c) the SLSC beamformer were overlaid on the co-registered B-mode image. A photoacoustic response from the out-of-plane fiber appears below the seed.

3. RESULTS

One coated brachytherapy seed was implanted approximately 4 mm from the fiber, as shown in Fig. 1(a). It is difficult to visualize the seed in this ultrasound image due to its small size and poor acoustic contrast. The FFT-based photoacoustic image (Fig. 1(b)) enhances seed visualization, but there is a persistent level of background noise that decreases seed contrast. The seed is better visualized in the corresponding SLSC beamformed photoacoustic image (Fig. 1(c)). The SLSC beamformed image has less background noise than the FFT-based image when both photoacoustic images are shown with the same dynamic range. The laser energy for these images measured 3.5 mJ, which corresponds to an energy density of 48 mJ/cm^2 at the conical sheath tip.

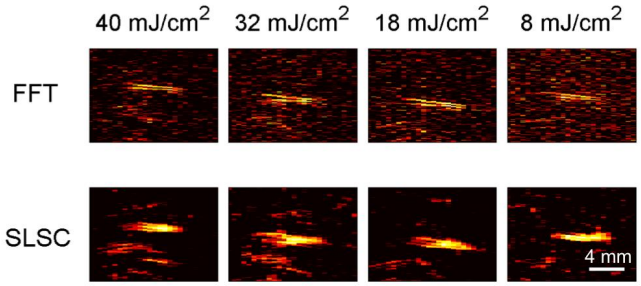

(a)

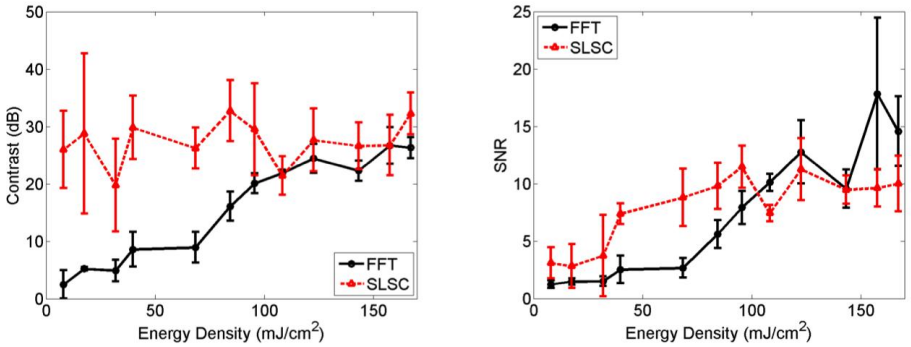

(b) (c)

Figure 2. (a) Comparison of FFT-based and SLSC photoacoustic images of the single coated brachytherapy seed shown in Fig. 1. Corresponding (b) contrast and (c) SNR measurements as a function of energy density at the sheath tip. Measurements were averaged over 3-5 trials. Error bars show ± one standard deviation.

The laser energy was varied from 8-40 mJ/cm^2 and corresponding photoacoustic images of the brachytherapy seed are shown in Fig. 2(a). The seed was increasingly difficult to visualize as laser energy decreased for the FFT-based images (top row). When SLSC imaging was implemented, the seed had better visibility with reduced background noise (bottom row). Seed contrast and SNR were measured for energy densities ranging 8-167 mJ/cm^2, as reported in Fig. 2(b) and (c), respectively. Results demonstrate that the SLSC beamformer has up to 22 dB improved contrast and similar or up to 4 times better SNR compared to the FFT-based images, particularly when laser energies were below the ANSI safety limit of 100 mJ/cm^2.

Two additional brachytherapy seeds were implanted in a different location of the *in vivo* canine prostate, as shown in Fig. 3(a). The corresponding SLSC and FFT-based photoacoustic images are shown in Fig. 3(b) and (c), respectively. The seeds were located at a distance of approximately 5 mm from the tip of the fiber. The seeds appear with image artifacts caused by a photoacoustic response from the tissue surrounding the fiber (red arrow) and acoustic reverberations between echogenic structures surrounding the source of the photoacoustic signals (yellow arrow). These artifacts are spatially coherent, and hence, the SLSC image fails to reduce them. In addition, these artifacts have similar amplitudes to the seed signals, thus a decrease in the dynamic range of the FFT-based image shown in Fig. 3(c) would diminish visualization of both the seeds and the artifacts.

The raw photoacoustic data (i.e. data acquired prior to beamforming or image reconstruction) was used to investigate the 2D frequency spectra of the image artifacts. The reverberation and fiber-related artifact had quadrantal symmetry. These spectra were different from that of the seed, which had diagonal symmetry and a negligible DC frequency component. Given the characteristic spatial frequency differences between the seeds and the spatially coherent image artifacts, a bandpass diagonal filter was applied to the photoacoustic data, prior to FFT-based reconstruction. The resulting image is shown in Fig. 3(d). The fiber- and reverberation-related artifacts were reduced by 9 and 14 dB, respectively, in the filtered image when compared to the unfiltered FFT-based image.

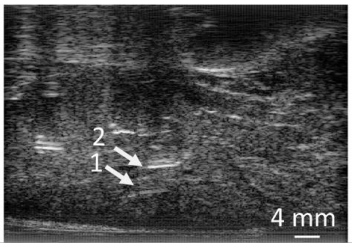

(a)

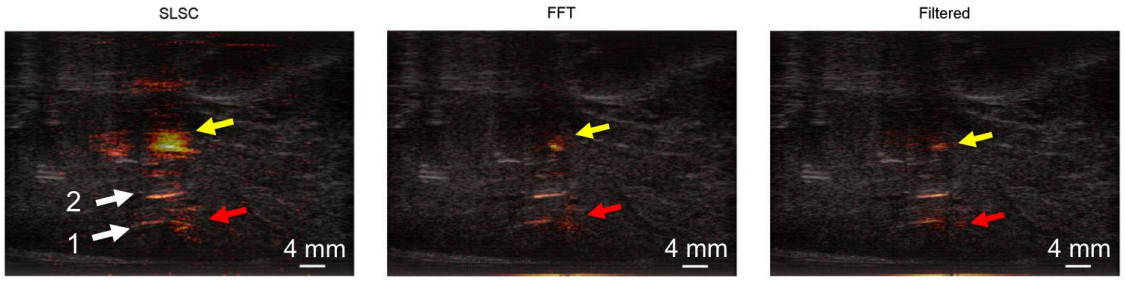

(b) (c) (d)

Figure 3. (a) Ultrasound B-mode image and corresponding (b) SLSC and (c) FFT-based photoacoustic images of two brachytherapy seeds implanted in the canine prostate. The photoacoustic images are overlaid on the co-registered ultrasound image. The photoacoustic images show artifacts due to the fiber location (red arrow) and acoustic reverberation (yellow arrow). (c) These artifacts were reduced by applying a bandpass diagonal filter prior to FFT-based image reconstruction.

4. DISCUSSION

The SLSC beamformer is ideal for reducing background noise that is spatially incoherent when performing photoacoustic imaging within the ANSI laser safety limit of 100 mJ/cm^2 for a 1064 nm laser wavelength. Low-contrast FFT-based photoacoustic images were enhanced with the SLSC beamformer within 8-84% of this limit. Thus, the SLSC beamformer offers a method to image seeds with high contrast at low laser energies, and thereby minimizes any potential risk of prostate tissue damage caused by the interstitial light delivery mechanism.

In vivo application of the SLSC beamformer provided average seed contrasts that were improved by up to 22 dB compared to the FFT-based reconstruction method, which is consistent with improvements achieved when the SLSC beamformer was compared to a conventional delay-and-sum beamformer.[11,12] These improvements are expected because the delay-and-sum beamformer and the FFT-based reconstruction method are both dependent on signal amplitudes, which are directly proportional to the laser energy. Combinations of coherence- and amplitude-based reconstruction methods might also be considered to achieve optimal image quality.

One limitation of the SLSC beamformer applied to seed detection is the amplification of artifacts that are spatially coherent (e.g. the reverberation and fiber-related artifacts shown in Fig. 3(b)). However, the 2D frequency spectra of these artifacts exhibited different symmetry compared to that of the seeds. These differences in frequency spectra may potentially be utilized to design advanced filters that remove these artifacts prior to coherence-based beamforming. In addition, photoacoustic image information can be integrated with existing ultrasound B-mode information to further reduce the unwanted artifacts, as the brachytherapy seeds will generally have spatial features (e.g. shape, size) that differ from those of the artifacts.

5. CONCLUSIONS

For the first time, we compare the SLSC beamformer to FFT-based reconstruction methods for detecting prostate brachytherapy seeds *in vivo*. The SLSC beamformer yields greater contrast and SNR compared to traditional FFT-based methods, and it is ideal for removing spatially-incoherent noise artifacts. Yet, it fails to reduce the spatially-coherent artifacts caused by a photoacoustic response at the fiber tip or acoustic reverberations between echogenic structures in the image field. Variations in the symmetry of the frequency spectra hold promise for advanced filtering methods to remove these spatially-coherent artifacts while preserving seed-related signals. Results indicate that advanced processing methods, such as coherence-based beamforming or frequency-based filters, play a critical role in the improvement of intraoperative seed localization with photoacoustic imaging.

ACKNOWLEDGMENTS

M. A. Lediju Bell is supported by the Ford Foundation and UNCF/Merck Postdoctoral Research Fellowships. Additional funding was provided by the Johns Hopkins Department of Radiology and NIH CA180561.

REFERENCES

[1] PJ Hoskin. Prostate cancer: permanent low dose rate seed brachytherapy and temporary high dose rate afterloading brachytherapy. *Radiotherapy in Practice-Brachytherapy*, page 103, 2011.

[2] J Crook. The role of brachytherapy in the definitive management of prostate cancer. *Cancer/Radiothérapie*, 15(3):230–237, 2011.

[3] JL Su, RR Bouchard, AB Karpiouk, JD Hazle, and SY Emelianov. Photoacoustic imaging of prostate brachytherapy seeds. *Biomedical optics express*, 2(8):2243, 2011.

[4] N Kuo, HJ Kang, DY Song, JU Kang, and EM Boctor. Real-time photoacoustic imaging of prostate brachytherapy seeds using a clinical ultrasound system. *Journal of biomedical optics*, 17(6):0660051–0660057, 2012.

[5] T Harrison and RJ Zemp. Coregistered photoacoustic-ultrasound imaging applied to brachytherapy. *Journal of Biomedical Optics*, 16(8):080502–080502, 2011.

[6] L Pan, A Baghani, R Rohling, P Abolmaesumi, S Salcudean, and S Tang. Improving photoacoustic imaging contrast of brachytherapy seeds. In *SPIE BiOS*, pages 85814B–85814B. International Society for Optics and Photonics, 2013.

[7] T Mitcham, K Homan, W Frey, YS Chen, S Emelianov, J Hazle, and R Bouchard. Modulation of photoacoustic signal generation from metallic surfaces. *Journal of biomedical optics*, 18(5):056008, 2013.

[8] CGA Hoelen, FFM de Mul, et al. Image reconstruction for photoacoustic scanning of tissue structures. *Applied Optics*, 39(31):5872–5883, 2000.

[9] KP Kostli, D Frauchiger, JJ Niederhauser, G Paltauf, HP Weber, and M Frenz. Optoacoustic imaging using a three-dimensional reconstruction algorithm. *Selected Topics in Quantum Electronics, IEEE Journal of*, 7(6):918–923, 2001.

[10] Y Xu, D Feng, and LV Wang. Exact frequency-domain reconstruction for thermoacoustic tomography. i. planar geometry. *Medical Imaging, IEEE Transactions on*, 21(7):823–828, 2002.

[11] MA Lediju Bell, N Kuo, DY Song, and EM Boctor. Short-lag spatial coherence beamforming of photoacoustic images for enhanced visualization of prostate brachytherapy seeds. *Biomedical Optics Express*, 4(10):1964, 2013.

[12] MA Lediju Bell, N Kuo, DY Song, JU Kang, and EM Boctor. In vivo photoacoustic imaging of prostate brachytherapy seeds. In *SPIE BiOS*. International Society for Optics and Photonics, 2014.

[13] MA Lediju Bell, AK Ostrowski, P Kazanzides, and EM Boctor. Feasibility of transcranial photoacoustic imaging for interventional guidance of endonasal surgeries. In *SPIE BiOS*. International Society for Optics and Photonics, 2014.

[14] MA Lediju Bell, X Guo, DY Song, and EM Boctor. Photoacoustic imaging of prostate brachytherapy seeds with transurethral light delivery. In *SPIE BiOS*. International Society for Optics and Photonics, 2014.

[15] BE Treeby and BT Cox. k-Wave: MATLAB toolbox for the simulation and reconstruction of photoacoustic wave fields. *Journal of biomedical optics*, 15(2):021314, 2010.

[16] MA Lediju, GE Trahey, BC Byram, and JJ Dahl. Short-lag spatial coherence of backscattered echoes: Imaging characteristics. *IEEE Transactions on Ultrasonics, Ferroelectrics and Frequency Control*, 58(7):1337, 2011.